A room-temperature mid-infrared photodetector for on-chip molecular vibrational spectroscopy

Bob Zheng, Hangqi Zhao, Ben Cerjan, Sadegh Yazdi, Emilie Ringe, Peter Nordlander, and Naomi J. Halas

Citation: Appl. Phys. Lett. **113**, 101105 (2018); doi: 10.1063/1.5045663
View online: https://doi.org/10.1063/1.5045663
View Table of Contents: http://aip.scitation.org/toc/apl/113/10
Published by the American Institute of Physics

A room-temperature mid-infrared photodetector for on-chip molecular vibrational spectroscopy

Bob Zheng,[1] Hangqi Zhao,[1] Ben Cerjan,[2] Sadegh Yazdi,[3,a)] Emilie Ringe,[3] Peter Nordlander,[1,2,3,4] and Naomi J. Halas[1,2,4,5,b)]
[1]*Department of Electrical and Computer Engineering, Rice University, 6100 Main St., Houston, Texas 77005, USA*
[2]*Department of Physics and Astronomy, Rice University, 6100 Main St., Houston, Texas 77005, USA*
[3]*Department of Materials Science and Nanoengineering, Rice University, 6100 Main St., Houston, Texas 77005, USA*
[4]*Laboratory for Nanophotonics, Rice University, 6100 Main St., Houston, Texas 77005, USA*
[5]*Department of Chemistry, Rice University, 6100 Main St., Houston, Texas 77005, USA*

(Received 22 June 2018; accepted 23 August 2018; published online 6 September 2018)

Infrared (IR) photodetection is of major scientific and technical interest since virtually all molecules exhibit characteristic vibrational modes in the mid-infrared region of the spectrum, giving rise to molecular spectroscopy and chemical imaging in this wavelength range. High-resolution IR spectroscopies, such as Fourier Transform IR spectroscopy, typically require large, bulky optical measurement systems and expensive photodetector components. Here, we present a high-responsivity photodetector for the mid-IR spectral region which operates at room temperature. Fabricated from silicon and aluminum, the photodetection mechanism is based on free carrier absorption, giving rise to a photoresponse rivalling commercially available cooled IR photodetectors. We demonstrate that infrared spectra of molecules deposited on this detector can be obtained by a direct electrical readout. This work could pave the way for simple, fully integrated chemical sensors and other applications, such as chemical imaging, which would benefit from the combination of mid-IR detection, room-temperature operation, and ultracompact portability. *Published by AIP Publishing.*
https://doi.org/10.1063/1.5045663

The quest for small, portable IR spectrometers has resulted in substantial miniaturization for the visible or near-IR spectral regions[1–3] but less for the mid-IR, largely due to the need for cryogenic cooling of IR detectors. Alternative spectroscopic systems utilizing nonlinear up-conversion techniques[4,5] have limited tuning ranges and have not been shown to be useful for general IR spectroscopy. Room-temperature IR sensors are generally more suited for thermal imaging than spectroscopy, with maximum sensitivities in the 8–10 μm spectral range.[6,7] State-of-the-art approaches with alternative IR materials, such as gapless 2D materials (e.g., graphene)[8–12] and colloidal quantum dots (CQDs),[13,14] utilize internal gain to increase photocurrent responsivity ($>$1 A/W) but generally have not yet been used for molecular detection. A sensitive, uncooled detector pixel for the mid-IR which uses earth-abundant materials and easily integrates into complementary metal oxide semiconductor (CMOS) fabrication processes would substantially improve upon existing photodetectors for this spectral range.

Our device structure [Fig. 1(a)] is based on combining the optical properties of periodic metallic nanostructures in the mid-IR range with a surprising mid-IR absorber: silicon. While intrinsic silicon typically exhibits high transparency in the mid-IR ($>$99%), doped silicon is a strong absorber of mid-IR light.[15] The mechanism for this strong absorption comes from the excitation of free holes (or electrons) near the band edges into unoccupied valence (or conduction) band states, known as free carrier absorption (FCA).[16,17] This absorption remains relatively constant from 4 K to 300 K (Ref. 16) and absorbs over a large spectral region, from the mid-infrared to the THz. These excitations have been used for far-IR and THz photodetection in the scheme known as μ-photoconductivity.[18,19] In this work, we demonstrate that this effect can also be used to detect mid-IR light. The boron-doped p-type substrate used here absorbs nearly 100% of mid-IR light within a thickness of 300 μm (Fig. S1). Additionally, the detector presented in this paper can be used for the direct electrical readout of molecular vibrational signals.

This detector is based on plasmonic gratings which have previously found broad applicability in a number of scientific disciplines,[20–23] especially in mid-IR applications,[24,25] due to their low optical losses in this spectral region and to the ease of tailoring their optical response through computational design. While plasmonic nanostructures have applications in mid-IR sensing,[26–30] plasmonic sensors demonstrated thus far must still be coupled to conventional optical systems to resolve their wavelength-dependent response. In the device design demonstrated here, the plasmonic grating strongly couples to IR light, enhancing the collection of incident light from the far field and serving two functions: as an electrical contact and as an IR-transmissive optical element.

The detector is composed of an aluminum metallic grating and a doped p-type silicon substrate. All devices were fabricated using standard complementary metal oxide semiconductor (CMOS) cleanroom fabrication techniques.

a)Present address: Renewable and Sustainable Energy Institute, University of Colorado-Boulder, Boulder, CO 80309, USA.
b)Author to whom correspondence should be addressed: halas@rice.edu

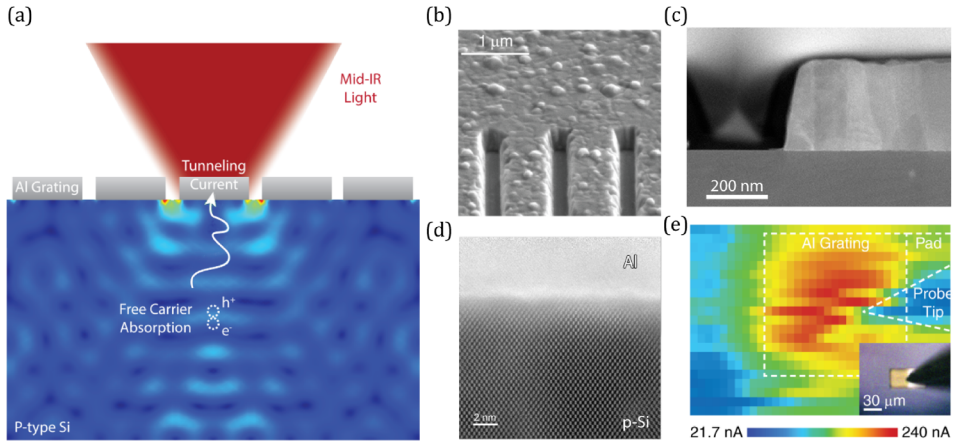

FIG. 1. Schematic and characterization of a photodetector. (a) Schematic illustration of a photodetector that generates a photoresponse based on the change in resistivity due to free carrier absorption. Silicon acts as an efficient IR absorber layer, while the metal antenna couples strongly to mid-IR light. The metal antenna serves as both a transmission window and an electrical contact. The calculated field distribution in silicon shows areas of higher FCA. (b) Scanning electron microscopy (SEM) image of an aluminum grating structure on a silicon substrate. The image was taken at 52° tilt. (c) Cross-sectional annular dark field scanning transmission electron microscopy (ADF-STEM) image of the structure and (d) a close-up of the Al-Si interface. (e) Photoresponse map of the representative device in (b). The inset shows a bright-field microscopy image of the approximate scanning area.

The metallic gratings are fabricated using electron beam lithography, metal evaporation, and lift-off. The active area is 30 μm by 30 μm with an overall pixel size of 30 μm $\times$ 60 μm. The grating thickness is $\sim$300 nm, and the gap size is kept at a constant 20% of the overall pitch (e.g., 200 nm for 1000 nm pitch) (for more information about device dimensions, see the supplementary material).

A scanning electron microscopy (SEM) image of a device fabricated with a 1 μm grating pitch is shown in Fig. 1(b) along with a cross-sectional annular dark field scanning transmission electron microscopy (ADF-STEM) image of the grating in Fig. 1(c). An atomic resolution cross-sectional ADF-STEM image of the device shows an atomically sharp interface between aluminum and silicon [Fig. 1(d)]. These two materials form a uniform contact without any noticeable diffusion or spiking (Figs. S3 and S4). The devices showed linear, ohmic current-voltage (IV) characteristics and no more than 20% device-to-device variability (Fig. S5).

The metallic grating significantly enhances the electrical response, observed through photoresponse mapping of the device. A mid-IR laser spot (4 μm laser wavelength, $\sim$10 μm spot size, 661 μW average power, and 200 fs pulse width) was raster-scanned over the sample, while the photoresponse, obtained at 0 V external bias (a small internal bias of 0.15 mV due to the lock-in amplifier is always present), is recorded at each spatial location [Fig. 1(e)]. A background FCA signal of $\sim$21.7 nA was observed. However, the measured signal (240 nA) significantly increases when the grating is directly illuminated.

The photodetector was used to directly measure the absorption resonances of films of polyvinylpyrrolidone (PVP) or poly(methyl methacrylate) (PMMA) at room temperature. The characteristic absorption spectra are shown in Figs. 2(a) and 2(b), respectively. PVP exhibits two absorption resonances in the 2–4 μm wavelength region at 2955 cm^{-1} and 3450 cm^{-1}, which correspond to -CH and -OH stretches, respectively.[31] PMMA has two closely spaced resonances, one at 2998 cm^{-1} and one at 2952 cm^{-1}, due to -CH_3 and -CH_2 stretching, respectively.[32] To obtain an electrical read-out of the absorption signal, the mid-IR laser light source is tuned from 2 μm to 4 μm in wavelength and the photoresponse is recorded with and without the polymer films. The difference between the two signals reproduces the spectral peak locations and relative peak absorption intensities for PVP and PMMA films obtained using a commercial Fourier Transform IR (FTIR) system.

The physics of this device can be described by first considering the Si band structure [Fig. 3(a)]. The band structure

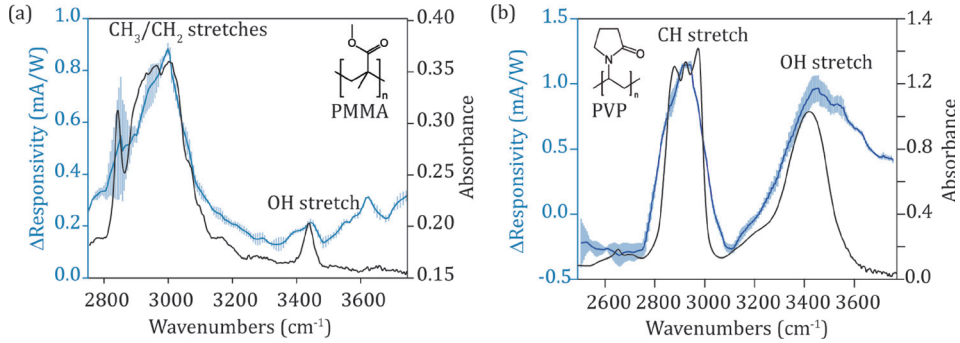

FIG. 2. Photodetector performance and direct electrical readout of absorption spectra. Measured changes in the photoresponse responsivity when a photodetector is coated with either (a) polyvinylpyrrolidone (PVP) or (b) poly(methyl methacrylate) (PMMA) are shown. The measured responsivities are overlaid with absorbance spectra obtained using a commercial FTIR system. The photodetector can clearly resolve the CH_2/CH_3, OH, and CH stretching modes of these two different polymers. The OH stretch in PVP is due to water. The error bars indicate the standard error.

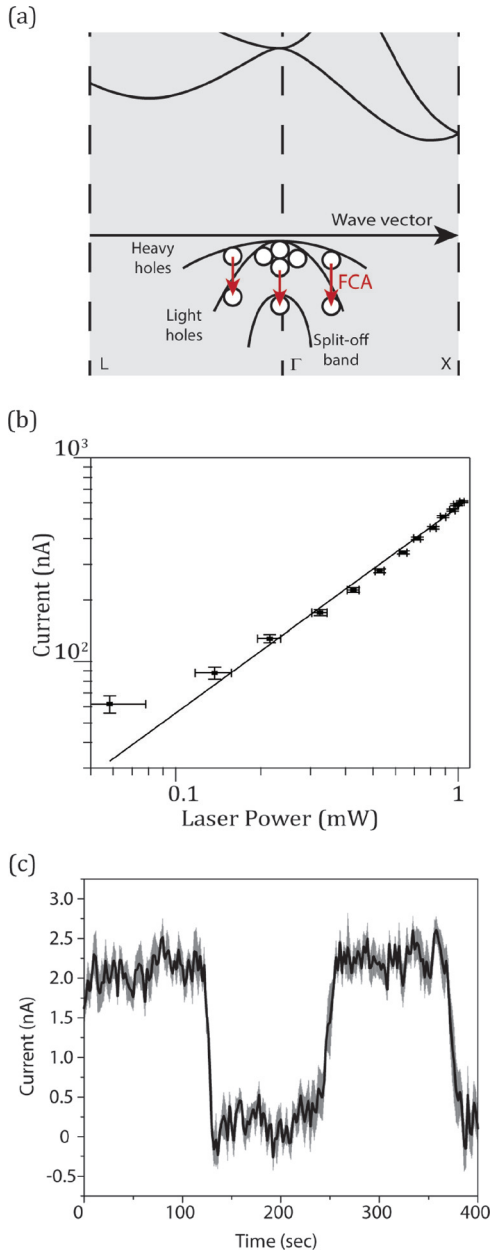

FIG. 3. Mechanism for the photoresponse. (a) Band diagram schematic of silicon showing the transitions in the valence band which correspond to FCA absorption. The effective mass of the holes in the light hole level and the split-off band decreases, resulting in higher hole mobility. (b) Current as a function of laser power showing a linear relationship between incident power and measured current. (c) Photoresponse using a blackbody source with a bandpass filter centered at 5 μm with a 0.5 μm FWHM, alternating turning on and off the source ($\sim$5 mW over the entire chip and $\sim$1.25 μW on the grating), 1375 nm pitch. The error bars denote the standard error. Note that the curve has been shifted by 2 nA to align the dark level with zero current.

shows that the transition from a heavy hole level to a light hole level or a split-off hole level results in carriers with a smaller effective mass, yielding higher mobility. For heavy holes, the effective mass is $0.49m_0$, while for light holes and split-off holes, it is $0.16m_0$ and $0.29m_0$, respectively.[33] This implies that photoexcitation of carriers will produce a change in device resistance, which can then be measured as a change in current through the device (for a fixed applied voltage). That the device shows a linear response when illuminated using both a laser source [Fig. 3(b)] and a blackbody source (Fig. S6) rules out possible contributions to the measured current from nonlinear up-conversion, as has been seen in some devices.[34,35]

This hypothesis is supported by two detector characteristics. First, the measured photoresponse of the device using a blackbody illumination source restricted to a spectral window of $\sim$4.75–5.25 μm ($\sim$5 mW over the entire chip) not only demonstrates the long wavelength response of the device but also rules out any nonlinear optical/ultrafast phenomena as the source of the measured current [Fig. 3(c)]. Second, finite-difference time-domain (FDTD) simulations demonstrate that neither the absorbed power nor the integrated electric field intensity in the first 100 nm of the silicon accurately reproduces our experimental data (Fig. S7). Instead, the transmitted power through the grating, or bulk silicon absorption, reproduces the experimental observations. This was confirmed by measurements, illuminating the side of a grating pad (Fig. S8) rather than the grating itself, indicating that the grating acts primarily as a spectral filter of the incident light. Additionally, measurements made on n-type Si with the same doping concentration showed no measurable photoresponse, indicating that the response is primarily due to the valence band structure of the silicon.

Further validation of the photodetector's current generation mechanism comes from correlating experimental responsivities over a range of grating pitches with their respective theoretical grating transmission. Devices with metallic gratings whose pitches are varied from 750 nm to 2000 nm were fabricated, and their responsivity was measured [Fig. 4(a)]. The wavelength dependence of the experimentally obtained photoresponses for these devices shows excellent agreement between the responsivity, the absorbance spectra obtained using Fourier Transform IR (FTIR) spectroscopy, and the calculated transmission for all measured devices [Fig. 4(b)]. The ability to design *a priori* the spectral bandwidth and shape of a Si-based, CMOS-compatible photodetector in the mid-IR allows for the possibility of large-scale integration into other detection schemes, such as compact hyperspectral imaging systems, and could potentially lead to mid-IR imaging systems at substantially lower costs than current technologies.

In summary, we have demonstrated a compact, uncooled photodetector for the mid-IR spectral region fabricated using aluminum and p-type silicon. The mechanism for photodetection is based on the modulation of electrical conductivity due to FCA in silicon. While this work focused on the 2–4 μm spectral region, the range of our tunable IR light source, a longer wavelength photoresponse can also be detected using a filtered blackbody source. These results indicate that this photodetector could readily be adapted to work at even longer wavelengths, particularly since FCA in Si occurs throughout the IR spectral region and has even been observed and used as a detection scheme at terahertz frequencies.[16,18] Additionally, as these detectors can be fabricated using conventional CMOS technology, can operate at room temperature, and can be made ultra-compact, they have the potential to be adapted to a wide array of IR devices. From focal plane arrays for microscale chemical mapping and imaging to fully integrated on-chip spectrometers,

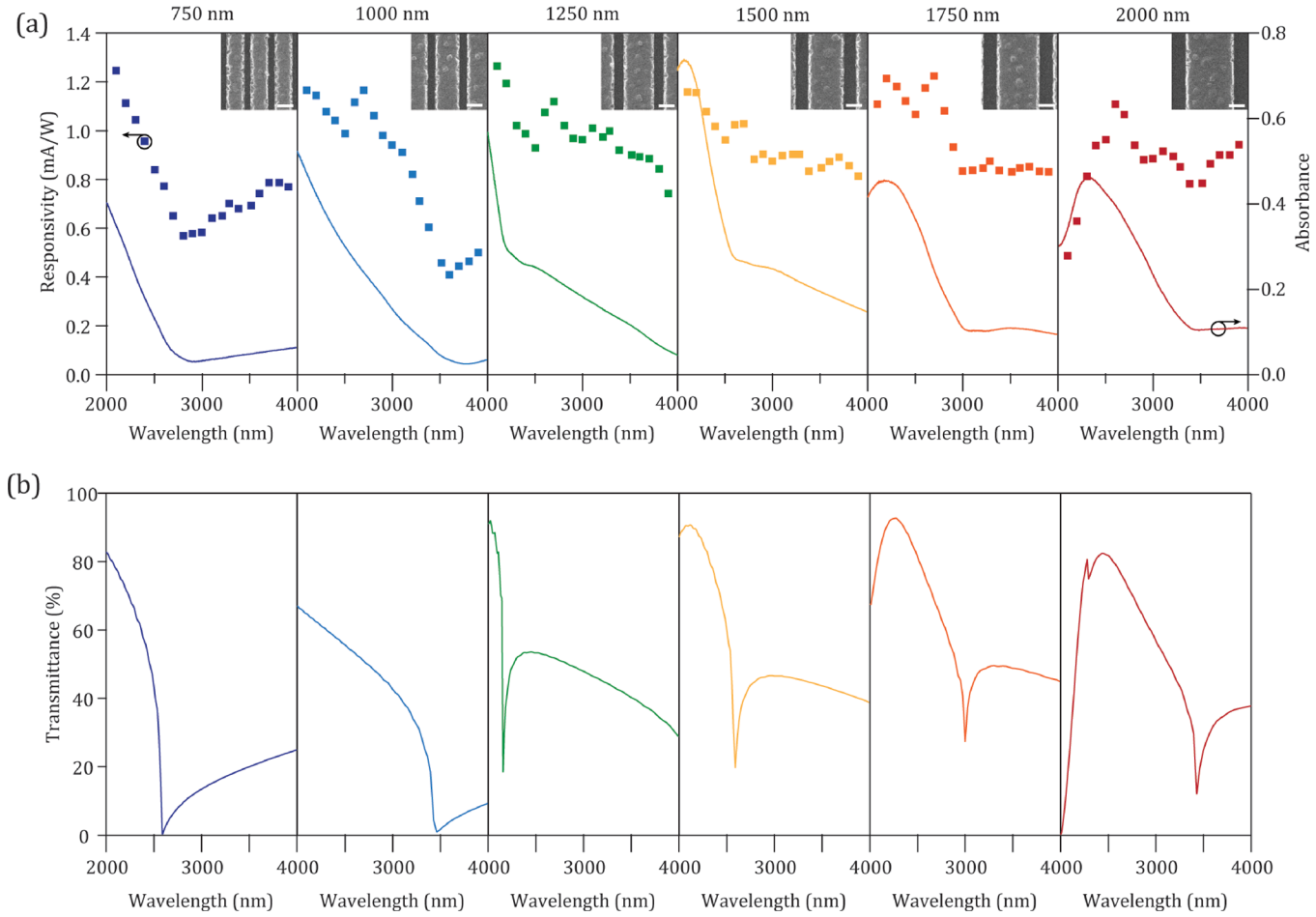

FIG. 4. Correlating measurements with theoretical calculations. (a) Measured optoelectronic response of the photodetector. Incident radiation is polarized perpendicularly to the grating direction. The responsivity (solid squares) is plotted with the measured absorbance (solid line), taken using Fourier transform IR spectroscopy (FTIR). The different colors correspond to different grating pitch distances. The inset shows the scanning electron microscopy images of the gratings, and the scale bar is 500 nm. (b) Calculated transmission spectra through the grating structure.

the device and mechanism presented here have potential in a wide range of applications.

See supplementary material for details about the sample fabrication, characterization, and optoelectronic measurements, along with additional simulation results, and further electrical characterization.

This work was supported by the Robert A. Welch Foundation under Grant Nos. C-1220 (N.J.H.) and C-1222 (P.N.), the Army Research Office under Grant No. W911NF-12-1-0407, the National Science Foundation (NSF) under Grant No. ECCS-1610229, the Air Force Office of Scientific Research Multidisciplinary Research Program of the University Research Initiative (AFOSR MURI FA9550-15-1-0022), and the Defense Threat Reduction Agency (DTRA) under Grant No. HDTRA1-16-1-0042.

[1]R. F. Wolffenbuttel, IEEE Trans. Instrum. Meas. **53**, 197 (2004).
[2]E. Laux, C. Genet, T. Skauli, and T. W. Ebbesen, Nat. Photonics **2**, 161 (2008).
[3]J. Bao and M. G. Bawendi, Nature **523**, 67 (2015).
[4]J. S. Dam, P. Tidemand-Lichtenberg, and C. Pedersen, Nat. Photonics **6**, 788 (2012).
[5]D. A. Kalashnikov, A. V. Paterova, S. P. Kulik, and L. A. Krivitsky, Nat. Photonics **10**, 98 (2016).
[6]P. Martyniuk and A. Rogalski, Opto-Electron. Rev. **21**, 239 (2013).
[7]A. Tittl, A. K. U. Michel, M. Schäferling, X. Yin, B. Gholipour, L. Cui, M. Wuttig, T. Taubner, F. Neubrech, and H. Giessen, Adv. Mater. **27**, 4597 (2015).
[8]X. Gan, R.-J. Shiue, Y. Gao, I. Meric, T. F. Heinz, K. Shepard, J. Hone, S. Assefa, and D. Englund, Nat. Photonics **7**, 883 (2013).
[9]B. Y. Zhang, T. Liu, B. Meng, X. Li, G. Liang, X. Hu, and Q. J. Wang, Nat. Commun. **4**, 1811 (2013).
[10]H. Yan, X. Li, B. Chandra, G. Tulevski, Y. Wu, M. Freitag, W. Zhu, P. Avouris, and F. Xia, Nat. Nanotechnol. **7**, 330 (2012).
[11]Y. Yao, R. Shankar, P. Rauter, Y. Song, J. Kong, M. Loncar, and F. Capasso, Nano Lett. **14**, 3749 (2014).
[12]C.-H. Liu, Y.-C. Chang, T. B. Norris, and Z. Zhong, Nat. Nanotechnol. **9**, 273 (2014).
[13]S. Keuleyan, E. Lhuillier, V. Brajuskovic, and P. Guyot-Sionnest, Nat. Photonics **5**, 489 (2011).
[14]E. Lhuillier, S. Keuleyan, P. Rekemeyer, and P. Guyot-Sionnest, J. Appl. Phys. **110**, 033110 (2011).
[15]R. Soref and B. Bennett, IEEE J. Quantum Electron. **23**, 123 (1987).
[16]D. K. Schroder, R. N. Thomas, and J. C. Swartz, IEEE J. Solid-State Circuits **13**, 180 (1978).
[17]D. K. Schroder, *Semiconductor Material and Device Characterization* (Wiley, 2006).
[18]S. Ganichev and W. Prettl, *Intense Terahertz Excitation of Semiconductors* (Oxford University Press, 2007).
[19]E. V. Beregulin, P. M. Valov, S. M. Ryvkin, D. V. Tarkhin, and I. D. Yaroshetskiĭ, Sov. J. Quantum Electron. **8**, 797 (1978).
[20]S. A. Maier, *Plasmonics: Fundamentals and Applications* (Springer US, Boston, MA, 2007).
[21]L. Wen, F. Sun, and Q. Chen, Appl. Phys. Lett. **104**, 151106 (2014).
[22]N. Yu, Q. J. Wang, M. A. Kats, J. A. Fan, S. P. Khanna, L. Li, A. G. Davies, E. H. Linfield, and F. Capasso, Nat. Mater. **9**, 730 (2010).

[23]R. Gillibert, M. Sarkar, J. Moreau, M. Besbes, M. Canva, and M. L. De La Chapelle, J. Phys. Chem. C **120**, 27562 (2016).
[24]R. Stanley, Nat. Photonics **6**, 409 (2012).
[25]S. Law, V. Podolskiy, and D. Wasserman, Nanophotonics **2**, 103 (2013).
[26]C. Wu, A. B. Khanikaev, R. Adato, N. Arju, A. A. Yanik, H. Altug, and G. Shvets, Nat. Mater. **11**, 69 (2012).
[27]L. V. Brown, K. Zhao, N. King, H. Sobhani, P. Nordlander, and N. J. Halas, J. Am. Chem. Soc. **135**, 3688 (2013).
[28]D. Rodrigo, O. Limaj, D. Janner, D. Etezadi, F. J. Garcia de Abajo, V. Pruneri, and H. Altug, Science **349**, 165 (2015).
[29]F. Le, D. W. Brandl, Y. A. Urzhumov, H. Wang, J. Kundu, N. J. Halas, J. Aizpurua, and P. Nordlander, ACS Nano **2**, 707 (2008).
[30]B. Schwarz, P. Reininger, D. Ristanić, H. Detz, A. M. Andrews, W. Schrenk, and G. Strasser, Nat. Commun. **5**, 4085 (2014).
[31]A. Slistan-Grijalva, R. Herrera-Urbina, J. F. Rivas-Silva, M. Ávalos-Borja, F. F. Castillón-Barraza, and A. Posada-Amarillas, Mater. Res. Bull. **43**, 90 (2008).
[32]B. Schneider, J. Štokr, P. Schmidt, M. Mihailov, S. Dirlikov, and N. Peeva, Polymer (Guildf) **20**, 705 (1979).
[33]B. Van Zeghbroeck, *Principles of Semiconductor Devices* (Colorado University, 2004).
[34]S. Zlatanovic, J. S. Park, S. Moro, J. M. C. Boggio, I. B. Divliansky, N. Alic, S. Mookherjea, and S. Radic, Nat. Photonics **4**, 561 (2010).
[35]J. Leuthold, C. Koos, and W. Freude, Nat. Photonics **4**, 535 (2010).